Measurement 259 (2026) 119667

Contents lists available at ScienceDirect

Measurement

journal homepage: www.elsevier.com/locate/measurement

Impact of cellularity in the flame front on the burning velocity acceleration of ethanol/air flames in constant volume combustion bomb☆

Miriam Reyes [a], Rosaura Sastre [a,*], Hong-Quan Do [b], Luis Le Moyne [b]

[a] Department of Energy and Fluid Mechanics Engineering, University of Valladolid, Paseo del Cauce s/n, E-47011 Valladolid, Spain
[b] Université de Bourgogne Europe, DRIVE Lab, 49 rue Mademoiselle Bourgeois, 58000 Nevers, France

ARTICLE INFO

Keywords:
Ethanol
Burning velocity
Schlieren technique
Accelerations
Cellularity

ABSTRACT

The objective of this work was to characterize the impact of cellularity developed at the flame front on the burning velocity of ethanol/air flames in a constant-volume combustion bomb by varying the ethanol/air equivalence ratio (0.8–1.4), initial pressure (0.15–0.3 MPa) and initial temperature (343–373 K). Cellularity at the flame front was studied using instantaneous Schlieren images of flame morphology obtained with a high-speed camera. Results show that ethanol-air flames exhibit increased cellularity at the flame from as the equivalence ratio in rich mixtures ratio increases and with increasing initial pressure, thereby accelerating the burning velocity. Although acceleration of the burning velocity is observed in all experiments, not all of them develop in the same mode: there may be a relationship between the burning velocity profile and the type of cellularity (inherent instabilities) established at the flame front in each case. Three types of acceleration are considered and investigated: one-stage, two-stage and progressive acceleration. The flame front structure and the instabilities that give rise to the cellularity phenomenon during combustion may be important for understanding the transition to turbulent combustion. They also play a key role characterizing the increase in burning velocity and its acceleration in premixed flames, in comparison with laminar burning velocity obtained from kinetic modelling.

1. Introduction

Ethanol is a commonly used alternative fuel derived from renewable sources, primarily plants like corn, sugarcane and other types of biomass. Ethanol is also an attractive fuel with high octane number (RON/MON = 120/99) for spark-ignited internal combustion engines [1], and produces lower carbon emissions than fossil fuels. The burning of this renewable fuel should not lead to an increase in the total amount of greenhouse gases in the atmosphere, and it should decrease the formation of soot, CO and unburned fuel [2]. Thus, the fundamental combustion performance of ethanol needs to be well understood, especially under engine-relevant conditions.

The burning velocity of premixed flames is an important concept for the analysis, design and performance of internal combustion engines (ICE), because it affects the burn rate, heat release rate, exhaust emissions, engine efficiency, and is directly affected by the thermophysical properties of the fuel/air mixture. Burning velocities also play a critical role in the development, testing, and validation of combustion models, as well as in the verification of complex kinetic mechanisms [3]. A variety of experimental techniques have been employed to determine the laminar burning velocity (LBV) of ethanol/air flames. These include the counterflow twin-flame technique [4], the heat flux method [1–5], and the spherical explosion bomb method [6–9]. One of the primary advantages of using the spherical combustion bomb technique is that it not only allows the measurement of LBV at high pressures that closely resemble those found in internal combustion engines [10,11], but it also offers the opportunity to investigate how the instabilities that arise in the flame front affect the overall performance from the ethanol combustion process [6–9]. This is of particular importance because the inherent flame instabilities, which can be quite prominent, play a crucial role in internal combustion engines [12,13]. These instabilities influence various engine parameters and understanding them is vital since they can both improve engine efficiency and contribute to undesirable phenomena such as knocking [13–15]. Therefore, the study of these flame instabilities is essential for optimizing engine performance and

☆ This article is part of a special issue entitled: 'MEASUR_XXIV IMEKO World Congress' published in Measurement.

* Corresponding author.
E-mail addresses: miriam.reyes@uva.es (M. Reyes), rosaura.sastre@uva.es (R. Sastre), yujun.cao@u-bourgogne.fr (H.-Q. Do), luis.le-moyne_isat@u-bourgogne.fr (L.L. Moyne).

https://doi.org/10.1016/j.measurement.2025.119667
Received 27 June 2025; Received in revised form 7 November 2025; Accepted 9 November 2025
Available online 11 November 2025

Nomenclature

Latin symbols

T	Temperature [K]
r	Radius [m] or [cm]
A_f	Flame front area [m^2] or [cm^2]
a_{cell}	Cellular acceleration
k	Stretch rate
L	Markstein length
Le	Lewis number Le = α/D.
M	Molecular diffusivity
m	Mass [kg] or [g]
$\dot{m}_b$	Mass burning rate [kg/s]
N_{cells}	Number of cells
n_{vel}	Normalized burning velocity
n_{cell}	Normalized cellular density
S_f	Flame propagation speed (in spherical flames $S_f = dr/dt$) [m/s]
S_n	Stretched burning velocity [m/s]
S_l^0	Unstretched laminar burning velocity [m/s]
p	Pressure [MPa]

Greek symbols

α	Thermal diffusivity
ρ	Density [kg/m^3]
ρ_{cell}	Cellular density [number of cells/m^2]
δl	Flame front thickness
φ	Fuel/air equivalence ratio

Subscript symbols

cell	Cellular
Comb	Combustion
max	Maximum
i	Initial condition
f or flame	Referred to the flame
b	Referred to the gas burned
ub	Referred to the unburned gas

Acronyms

LBV	Laminar Burning Velocity [m/s]
CVCB	Constant Volume Combustion Bomb
ICE	Internal combustion engine
CBS	Cellular burning stage
CO	Carbon monoxide
DL	Darrieus-Landau
RON	Research Octane Number
MON	Motor Octane Number

mitigating issues like engine knocking.

There are three primary phenomena that can cause instabilities in the flame front of a premixed flame under laminar conditions: volume forces, hydrodynamic effects, and thermo-diffusive effects [16]. Volume forces become significant when a lighter fluid moves toward a heavier one in the opposite direction of a body force, such as gravity. This leads to a type of instability known as Rayleigh-Taylor instability [17]. In the context of flames, this occurs when the combustion products (which are less dense) rise into the unburned fresh mixture (which is denser), moving against gravity. Here, the flame front acts as a density discontinuity. Among the three mechanisms, volume force instabilities have the least influence on flame development.

The second type of instability is the hydrodynamic instability, also known as the Darrieus-Landau (DL) instability. It arises from thermal expansion or density difference between the unburned and burned gases across the flame front [14,18]. This instability is inherently destabilizing, as it amplifies perturbations on the flame front that are significantly larger than the flame front thickness (δ_l) [16,19]. Hydrodynamic instability is promoted by thinner flame fronts and elevated pressures [20]. Moreover, its onset can lead to an increase in turbulent flame propagation speed [21,22].

The third type of instability is driven by thermo-diffusive effects, which play a significant role in the combustion process. Unlike hydrodynamic or volume force instabilities, thermo-diffusive instability does not consistently stabilize or destabilize, as it results from the interplay between thermal and molecular diffusivities, which have opposing influences [16,23–26]. Molecular diffusivity tends to amplify perturbations in the flame front, contributing to destabilization, while thermal diffusivity works to smooth out these perturbations, exerting a stabilizing effect. This balance can be quantitatively described using the dimensionless Lewis number (Le), which is the ratio between thermal diffusivity (α) and molecular diffusivity (D), $Le = \alpha/D$.

Thermo-diffusive instability becomes destabilizing when the Lewis number falls below a critical value—meaning molecular diffusivity dominates over thermal diffusivity. In this case, cracks and cellular structures can form immediately at the flame front. Otherwise, the flame initially remains smooth, and visible wrinkles only appear later, once hydrodynamic instabilities have had time to develop [27].

To understand thermo-diffusive instabilities in premixed flames—especially in fuels like ethanol—it is necessary to consider a few fundamental combustion properties that play a crucial role. These properties help determine flame stability and behaviour, particularly in relation to Markstein length (L), which is a key parameter for assessing flame response to perturbations. Markstein length can be defined as a measure of the effect of stretch rate (k) —i.e. curvature and strain— on burning velocity, $S_n = S_l^0 - L \cdot k$, where the S_l^0 is the unstretched laminar burning velocity and S_n is the stretched laminar burning velocity.

In addition, the influence of flame stretch must be considered in spherical flames. This factor encompasses both strain and curvature effects resulting from the flame's geometry, and it consistently acts to dampen instabilities during the early stages of combustion, reflecting the flame's inherently stable nature. Ethanol flames in reach mixtures have a Lewis number lower than 1, different from the methane with values around 1, and Markstein length for ethanol tends to be lower than that for methane, and is zero or negative in rich mixtures, indicating that fuel diffuses faster than heat.

In recent years, several studies have been published on flame instabilities in ethanol combustion processes. These investigations aim to better understand how various factors, including fuel composition and combustion conditions, influence flame stability, especially when ethanol is blended with other fuels. One area of particular interest is the interaction between ethanol and hydrogen in combustion systems. For example, a study by Li et al. [7] examined the effects of hydrogen content on the flame instability during hydrogen/ethanol/air combustion. Their findings revealed that as the hydrogen ratio in the mixture increased, the premixed flame became more hydrodynamically unstable. This result highlights the significant role of hydrogen in altering combustion dynamics, as the added hydrogen changes the fuel's combustion characteristics, potentially leading to more complex and less stable flame behaviour. A significant study developed by Liu et al. [8] analysed the impact of initial temperature and pressure on the stability of E30 (a mixture consisting of 30 % ethanol and 70 % gasoline surrogate) flames in an air. In addition to examining the effect of temperature and pressure, this research also explored the types of instabilities that developed under varying conditions. The experimental and numerical results of this study indicated that the chemical effect of adding ethanol

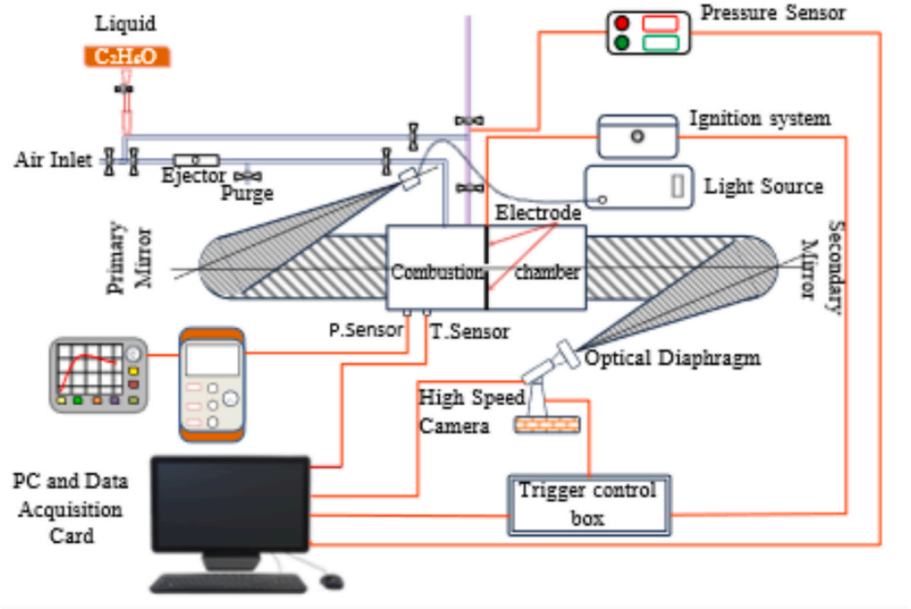

Fig. 1. Scheme of the experimental set-up.

Table 1
Test conditions for ethanol/air mixtures.

Parameter	Value
Initial pressure (p_i, bar)	(0.15–0.3) MPa
Initial temperature (T_i, K)	343 K
Equivalence ratio (ϕ)	0.8–1.4

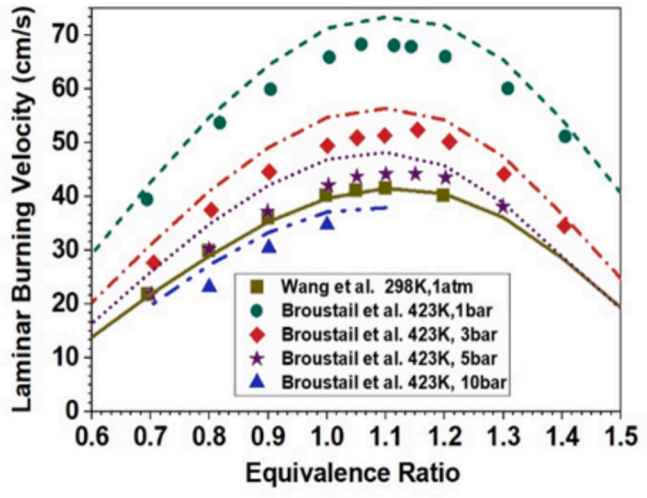

Fig. 2. Comparison of experimental [10,36] and calculated [27] LBVs of ethanol. (Symbol: experimental data. Line: numerical results).

to a TRF (Toluene Reference Fuel) mixture was greater than the thermal effect, meaning that the dominant influence of ethanol was through chemical interactions rather than through changes in the thermal properties of the mixture. Moreover, Liu et al. [8] observed that the flame instability behaviour was largely governed by variations in hydrodynamic instability, which are influenced by changes in initial pressure. As the pressure increased, the nature of the instabilities shifted, with the transition from simpler instability forms to more complex ones. In fuel-rich flames, the study revealed that the flame instability was primarily controlled by cellular instability, which is typically governed by diffusional-thermal instability [15]. This type of instability arises from the differences in diffusion rates of the fuel and oxidizer, combined with thermal gradients within the flame front. These findings are crucial for understanding how fuel composition and operating conditions, such as pressure and temperature, contribute to the overall combustion behaviour, especially when blending ethanol with gasoline or other fuels. These studies demonstrate the complexity of flame instability phenomena in ethanol combustion, emphasizing the need to consider both chemical and physical factors when analysing combustion systems. The influence of ethanol on flame stability is not just a matter of thermal effects but also involves significant chemical reactions that alter the combustion characteristics, and understanding this interaction is essential for optimizing combustion efficiency and minimizing undesirable phenomena such as knocking and incomplete combustion.

Other studies have also examined the behaviour of combustion processes when ethanol is used as the sole fuel. One such recent investigation by Garzón et al. [6] explored the effect of adding water on the instabilities at the ethanol flame front. Their findings highlighted that the equivalence ratio has a substantial influence on flame stability. In mixtures that were slightly fuel-rich, they observed the greatest tendency for hydrodynamic instabilities to develop. On the other hand, in richer mixtures, the flames were more prone to developing thermo-diffusive instabilities. Additionally, they found that initial pressure played a role in enhancing the thermo-diffusive instability, particularly in rich mixtures. In contrast, initial temperature had a relatively minor impact on the development of flame-front instabilities. These results align with the conclusions of a previous study by N. Zhang et al. [9] who presented a numerical and theoretical analysis of ethanol/air flame instabilities. However, despite the valuable insights provided by these studies, one important phenomenon related to ethanol flames has not yet been fully explored: the self-acceleration of ethanol flames. Although this concept has not been discussed extensively in the literature, it could potentially play a significant role in the transition from laminar to turbulent flame regimes [6]. This phenomenon merits further investigation, as understanding it could provide deeper insight into the dynamics of ethanol combustion and help optimize combustion processes in practical applications. Intrinsic instabilities (hydrodynamic and–-thermo-diffusive) can trigger self-acceleration by increasing the flame surface area, which, according to the literature, leads to a regime that can be defined as “turbulent” (Markstein [12], Matalon [14]). Huang et al. [28], demonstrated that in hydrogen flames self-acceleration is

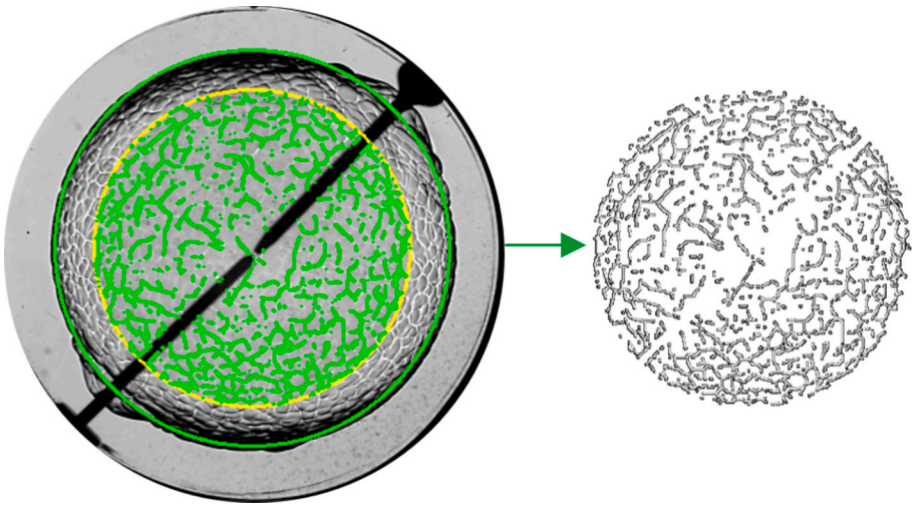

Fig. 3. Contour detection in Python using the "findContours" function, applied to identifying cellularity in the flame front of an ethanol flame with an equivalence ratio of 1.01, initial pressure of 0.3 MPa, and initial temperature of 343 K.

primarily driven by intrinsic instabilities under quiescent conditions (with no external turbulence), while turbulent eddies only become relevant when external turbulence is introduced. They also concluded that when turbulence is high, it suppresses the effects of intrinsic instabilities in the flame.

Therefore, the objective of the present study is to investigate the role of cellularity and the development of inherent instabilities in the apparent burning velocity of ethanol/air flames under various initial conditions of pressure, temperature, and equivalence ratio. The present study is based on previous work by Reyes et al. [29] on ethanol flames. The present work continues and extends that study to further investigate the consequences of cellularity in flames, especially regarding the acceleration of combustion processes, as a consequence of cellularity. The novelty of the present research is to characterize the acceleration originated in the burning velocity, by comparing the evolution of the burning velocity (obtained from the pressure trace and diagnosis model) and the cells (obtained with optical diagnosis). In this way, it is possible to distinguish the type of acceleration due to cellularity (with different stages), because of the variation in the heat release rate and turbulence, as a function of the ethanol/air equivalence ratio. To achieve this, the ethanol/air mixtures are tested in an experimental combustion setup, where the combustion behaviour is analysed under cellular conditions to determine the burning velocity. Subsequently, a kinetic model is used to calculate the laminar burning velocity (LBV) and to compare the results with the experimental findings. This approach will provide a deeper understanding of how these factors influence the combustion characteristics and the acceleration and morphology of ethanol/air flames.

2. Methodology

2.1. Experimental setup

A cylindrical, constant volume combustion bomb equipped with optical access was used for experimental testing. A schematic of the experimental setup is shown in Fig. 1. To investigate and characterize the impact of intrinsic instabilities on the appearance of cellularity, as well as on burning velocity and flame growth, ethanol/air mixtures are introduced into the cylindrical constant-volume combustion bomb. The progress of combustion and the flame-front evolution are tracked using the Schlieren technique [30]. In Table 1 the experimental conditions are displayed.

A cylindrical combustion vessel, constant-volume combustion bomb (CVCB), with a diameter of 114 mm and a length of 135 mm, is used to visualize the combustion process with two optical access on the cylinder sidewalls. The high-speed Schlieren imaging procedure records flame images with a high-speed camera Phantom V210 at 7000 frames per second (resolution 832 × 800 and exposure time of 10 ms). The system is also equipped to measure initial pressure using pressure transducers, initial temperature using thermocouples, and the instantaneous pressure during combustion using a piezoelectric pressure transducer Kistler type 7063 (maximum calibration error 0.06 %).

Air is introduced into the CVCB using the partial pressure method and ethanol fuel is introduced using calibrated micro syringes, once the initial conditions of pressure, temperature and equivalence ratio have been established. To ensure homogeneity, a spark plug ignites combustion at the geometric centre of the combustion vessel after five minutes of mixing. A spherical flame front then forms inside the CVCB and spreads outward.

An algorithm was developed in Python (Open CV) to process Schlieren images to analyse the images obtained with the high-speed camera, to characterise the evolution of the flame radius and to investigate the formation of the cellular structure on the flame-front surface. Additional information about the experimental setup is available in [31].

2.2. Burning velocity determination

In this section, results obtained from the ethanol/air mixtures are presented. Results presented of the burning velocity were obtained using three different methodologies: firstly, from the analysis of the instantaneous pressure recorded inside the CVCB, using a two-zone thermodynamic diagnostic model [32]; secondly, from recorded flame images [22], and thirdly, from kinetic modelling, which is explained in Section 2.3. The stretched burning velocity, S_n, is obtained from the temporal pressure trace during combustion and analysed with a two-zone thermodynamic diagnostic model, which simulates the CVCB and divides the combustion chamber into burned and unburned zones, applying of thermodynamic equations to both zones [33,34]. This model applies the definition of burning velocity detailed in Eq. (1), [30,32].

$$S_n = \frac{\dot{m}_b}{\rho_u \bullet A_f} \tag{1}$$

where $\dot{m}_b$ is the mass burning rate [kg/s], ρ_u is the density of the unburned gas [kg/m^3], and A_f is the area of the flame front [m^2].

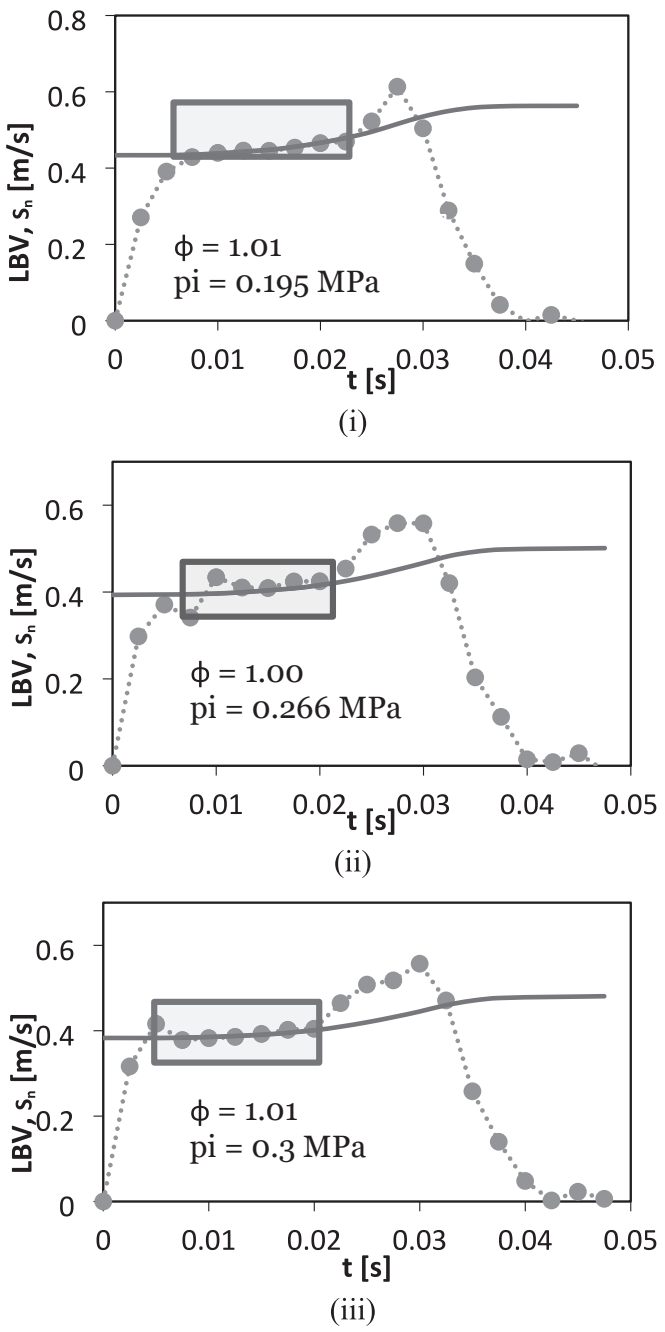

Fig. 4. Experimental stretched burning velocity and calculated LBVs for ethanol flames. (Symbol: experimental data. Line: LBV kinetic modelling results).

2.3. Kinetic modelling

The combustion reaction has been modelled with the CHEMKIN-PRO software package [35] in order to obtain the unstretched laminar flame propagation speed. The mechanism of Zhang et al. [27] developed for the low-temperature chemistry of ethanol has been implemented. This mechanism includes 433 species and 1004 reactions and has been shown to be effective for describing the chemical kinetics of ethanol oxidation at moderate and high temperatures. It was developed from ignition delay time measurements in rapid compression machine and in shock tubes covering lean to rich conditions (φ = 0.5, 1.0 and 2.0) over a wide temperature range (650–125 K) and under pressures from 20 to 40 bar. The CHEMKIN model used for this study retained a maximum of 1000 grid points, assuring grid independency in modelling the flame structure. The adjustment parameters, GRAD and CURV were both set to 0.05. The reactor model calculation was started at −2 cm and carried up to 10 cm.

As a preliminary step before carrying out the comparison between experimental data and model results, a validation of the laminar burning velocity (LBV) is performed. This validation is particularly important as high-pressure levels are investigated. It can be seen in Fig. 2 that the predictions and experimental data from two of the latest measurements of LVB for ethanol mixtures, using both the spherical flame method [10] and the heat flux method [36], and the results from the model chosen for this study are in good agreement. Model predictions are slightly lower, but the agreement is particularly satisfactory at atmospheric and elevated pressures. This mechanism has been validated against a wide range of experimental data (global and detailed) covering large temperature and pressure range. Zhou et al. [37] implemented it successfully in their study of laminar burning velocities of ethanol-air mixtures with hydrogen.

2.4. Self-acceleration phenomenon

The laminar burning velocity (LBV), ~~as~~ calculated using the kinetic modelling described in the previous section, represents an idealized value that does not account for certain phenomena inherent to combustion processes, such as instabilities and the resulting cellularity at the flame front. When cellularity is present, the burning velocity may differ significantly from the laminar burning velocity (LBV). This discrepancy arises from the increase in the flame surface area caused by the cellular structures, which, in turn, leads to an increase in the mass burning rate, $\dot{m}_b$ (see Eq. (1). Finally, this phenomenon results in what is commonly referred to as the self-acceleration of the process.

There are several studies that investigate the self-acceleration phenomenon in laminar flames, such as the one conducted by Omari et al. [38]. They compared the real propagation speed of the flame (flame speed, S_n) to the laminar propagation speed, obtained through a correlation, in flames of a hydrogen-methane mixture. They obtained an increase in the speed once the onset of the cellularity occurred. Reyes et al. [32] observed in their study in hydrogen flames that the cellularity led to an apparent burning velocity greater than the laminar value, indicating an acceleration of the combustion process. The self-acceleration effect has also been confirmed in several recent studies, which show the impact of the cellularity on both the burning velocity and flame speed [39–41].

2.5. Image processing

A new tool has been developed in Python using the "OpenCV" library for image processing, used to quantify cellularity in ethanol flames. The program counts the number of contours detected in the image using the function "findContours" provided by the library. To exclude the flame front and eliminate the influence of shadows, the program only evaluates the contours in a region corresponding to 80 % of the 2D area of the flame front, as shown in Fig. 3.

This approach is similar to the one suggested by Tinaut et al. [30], who presented an optical characterization of the cellularity in hydrogen-air laminar combustion processes.

3. Results and discussion

The present results and discussion follow and complement the results presented in a previous work developed by Reyes et al. [29] in 2025. In the present work a more detailed explanation of the burning velocity parameter is provided, along with a more precise description of the kinetic model used. New phenomena, such as self-acceleration, which is a consequence of the cellular flame structure, are described and analysed with image processing. Finally, a more thorough description of the

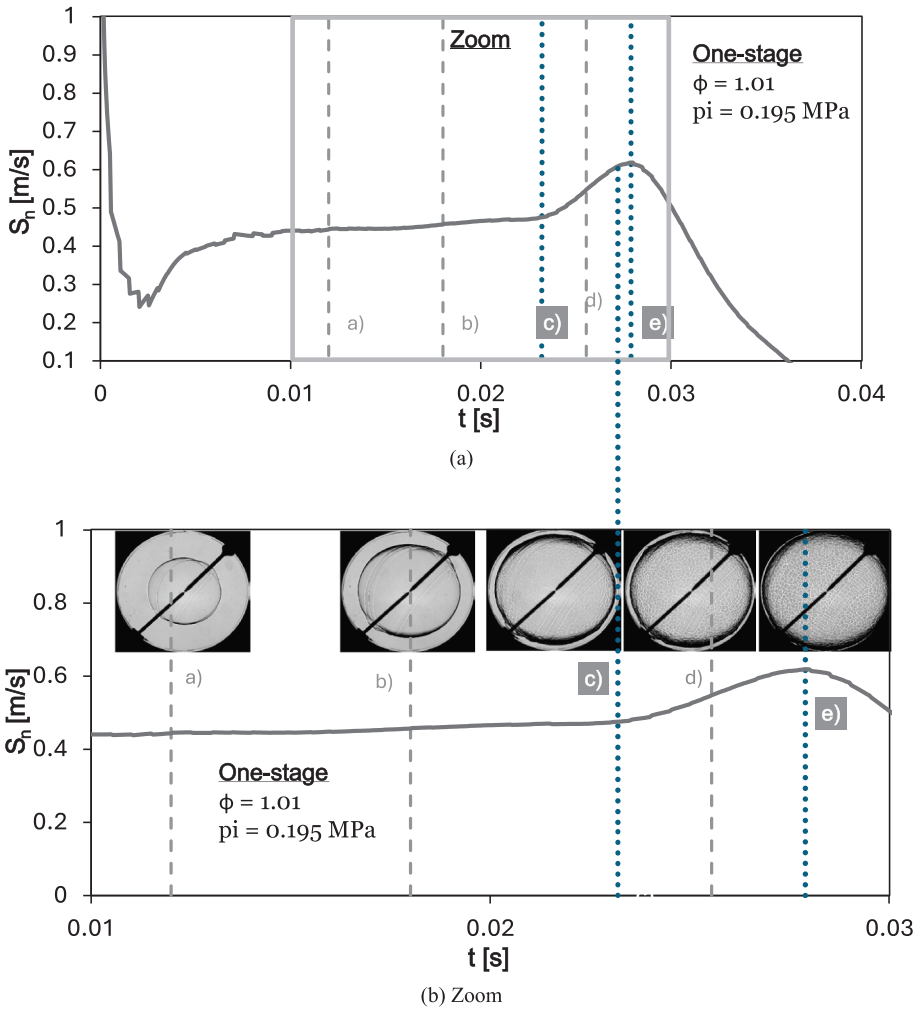

Fig. 5. Burring velocity for an ethanol flame with one-stage acceleration. Initial conditions: p_i = 0.1 MPa, T_i = 343 K and ϕ = 1.0.

different acceleration types observed in ethanol experiments is presented, including clearer technical naming for each category and examining the stages of the burning velocity acceleration, with new calculations and approaches, which have been completed using the results of the kinetic model previously explained.

3.1. Comparation between the kinetic modelling and experimental results

Experimental data derived from the analysis of the instantaneous pressure measured inside the CVCB, S_n, are compared with the LBV determined by kinetic modelling, to understand the effect of cellularity on laminar flames, Fig. 4. This approach provides valuable insight into the phenomena observed under different equivalence ratios and can be further developed in future studies to extend our understanding of flame acceleration mechanisms.

It is possible to study the effect of cellularity on burning velocity by categorizing and classifying the type of acceleration developed in the burning velocity. This classification defines the trend of the burning velocity due to the influence of inherent combustion instabilities. The aim is to establish a relationship between the laminar burning velocity and the real burning velocity of the processes by studying the increments in the burning velocity, and changes in flame morphology produced by different types of acceleration at the flame front. Based on the experiments defined in Table 1, three main types of acceleration have been observed. To illustrate each of them, experiments with the same initial pressure and temperature (0.19 MPa and 343 K), but at three equivalence ratios (1.01; 1.26; 1.4) are selected. In the following sections their burning velocity, as well as their morphological evolution are presented.

3.2. First type: one-stage acceleration

The first type is one-stage acceleration, and it is so named because it shows a sharp, single change in the flame front morphology and in the burning velocity (a single slope) once cellularity appears at the flame front. These combustion processes are characterized by an initial smooth and stable flame front, where any cracks that may form at the electrodes do not develop. After that, a clear transition to a cellular flame front is observed, where cellularity appears uniformly and homogeneously over the entire flame front surface without cells originating from electrode cracks. This can be identified by a clear and unique change in the slope of the burning velocity curve, as it can be seen in Fig. 5.

In Fig. 5 an example of ethanol combustion with initial conditions of 0.195 MPa, 343 K is presented, and an equivalence ratio of 1.01, which develops one-stage acceleration. The cellular radius, i.e. the radius at which the cellularity appears, is 5.219 cm in this case. Images are presented in a zoomed view in Fig. 5b. In this figure, the change in flame front morphology due to the appearance of cellularity—from b) to c)—can be clearly seen. This behaviour could be attributed to the hydrodynamic effect, based on the homogeneous aspect of the cells, as previously explained in Addabbo et al. [23].

Points c) and e) are highlighted because they correspond to the times at which the cellular flame front emerges and the maximum burning velocity is reached, respectively. In Fig. 5, it can be observed that points, c) and e), are connected by a single-slope curve, which gives this type of

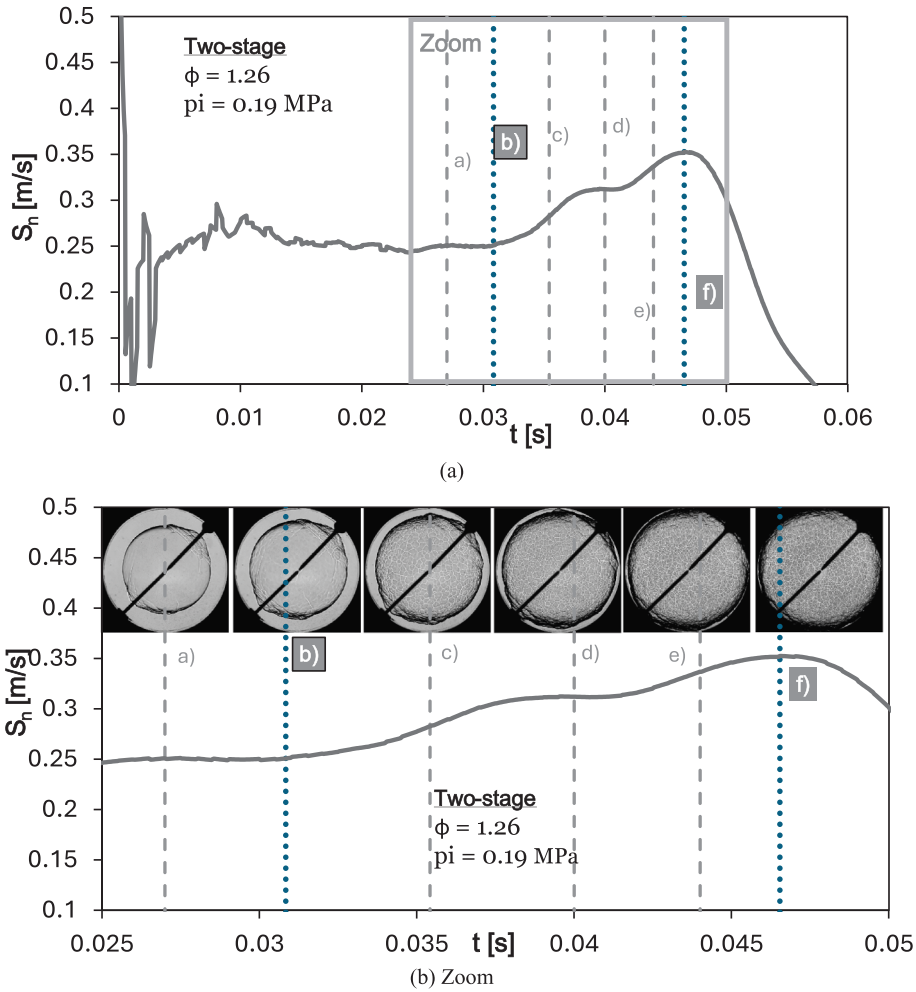

Fig. 6. Burring velocity for a combustion of ethanol with two-stage acceleration. Initial conditions: $p_i = 0.19$ MPa, $T_i = 343$ K and $\phi = 1.26$.

acceleration its name.

3.3. Second type: two-stage acceleration

The second type is the two-stage acceleration, and it is denominated as such because there are two distinct acceleration phases (two slope periods) after cellularity appears. To obtain this type of acceleration a richer equivalence ratio has been chosen: 1.26, as seen in Fig. 6. The first period of acceleration is very similar to that described in the one-stage acceleration: there is an initial rise in the burning velocity with a change in the flame morphology due to the onset of cellularity (the cells are homogenously spread all over the flame front), as seen in Fig. 6. After this initial acceleration phase, the burning velocity remains constant for a short period, as do the cells formed at the flame front in the first period. Afterwards, following this steady phase, the burning velocity increases again, and the initial cells spread out and divide into smaller ones (see Fig. 6). In this case the cellular radius is 4.554 cm. During the second acceleration phase, these initially formed cells divide and evolve into smaller ones near the end of the combustion process.

In summary, the first acceleration period or slope corresponds to the appearance of the cells on the flame front (onset of cellularity). Then there is a period in which the formed cells stabilize, and the burning velocity practically remains unchanged. In the second acceleration period, the initially formed cells divide again.

Fig. 6 shows how the main points b) and f) —which represent the onset of cellularity and the instant of maximum burning velocity, respectively— are connected by two acceleration periods (two single-slope curves). Instant a) represents the flame front before the onset of cellularity; instant c) represents the first period of acceleration, when the original cells are formed; instant d) represents the stabilization of the cells after the first period of acceleration; and instant e) represents the division of the original cells into smaller one (second period of acceleration).

3.4. Third type: progressive or multiple-stage acceleration

The last type is the progressive or multiple-stage acceleration, and in this work, it is observed at the richer equivalence ratio: 1.4. In this acceleration, cracks develop and intensify from the beginning of the combustion process, which can create closed regions of different sizes on a specific part of the flame. These closed regions do not spread out simultaneously over the surface of the flame because they are not considered to be cellularity. Due to the slow evolution of these closed regions and the initial cracks, a sharp change in the burning velocity trend is not clearly observed when cellularity appears over the entire flame (contrary to the other two types). The cellular radius is 5.463 cm. Instead, a more progressive change in the burning velocity and in the morphology of the flame is observed, hence the name of this type of acceleration, Also, the cells form between the cracks developed from the beginning, see Fig. 7.

In Fig. 7 it can be seen that, at the instants a) and b) there are already some initial cracks and closed regions on some parts of the flame surface, which occur before the onset of cellularity. When cellularity appears, the cells spread all over the surface of the flame, not just along a particular

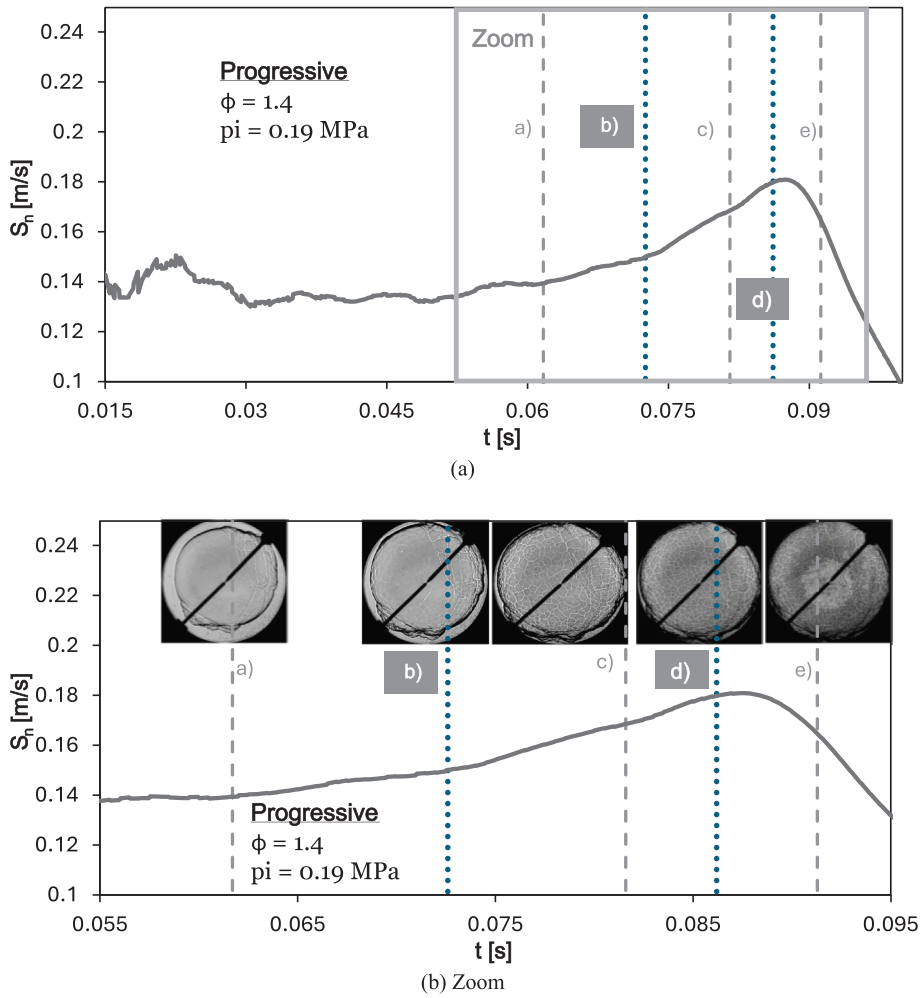

Fig. 7. Burring velocity for a combustion of ethanol with progressive acceleration. Initial conditions: p_i = 0.26 MPa, T_i = 343 K and ϕ = 1.4.

perimeter. As previously explained, these initially formed cracks and enclosed regions make the change in the burning velocity, more progressive than in the previous two types, therefore, the acceleration or the change in the trend of the burning velocity is not as abrupt than previously. In this type it can be observed a more heterogeneous and clustered cellularity, and it could be associated with the thermal-diffusive effect, as explained in Sastre et al. [42]. In Fig. 7, the main points b) and d) are connected by multiple periods of small accelerations, giving the appearance of a smooth and progressive slope.

These three experiments show that the type of acceleration depends strongly on the equivalence ratio: a near-equivalence ratio condition show one-stage type, a richer one has the two-stage type, and the richest condition provoke the progressive type.

3.5. Effect of cellularity on the laminar burning velocity

On the one hand, this section aims to demonstrate that the change in flame morphology due to cellularity is responsible for the acceleration of the burning velocity. On the other hand, it seeks to quantify the effect of cellularity on the burning velocity. To address the first purpose, the approach suggested involves the comparison between the burning velocity (u_n) and the morphological changes observed in the flame images. This requires the following steps:

a) Obtain a quantitative measure that represents the morphological changes in the flame caused by cellularity.

b) Normalize both the burning velocity and the quantitative measurement of the cellularity to enable a better comparation.

To obtain a quantitative measurement that represents the morphological changes (second purpose of this section) the image processing method described earlier is employed (see point "2.4. Image processing"). The output of the program is the number of contours, n_{cont}, detected in each frame during the combustion process. The parameter through which the evolution of the cellularity can be compared must be independent of the flame size. Tinaut et al. [30] defined a parameter called the "cellularity density index", which is the number of cells (N_{cells}) per unit area. In the present work the parameter is called "cellular density", ρ_{cell} and is calculated as shown in Eq. (2), where:

$$\rho_{cell} = \frac{N_{cells}}{A_{red}} = \frac{N_{cells}}{\pi \bullet (r \bullet 0.8)^2} \tag{2}$$

Once the first step is completed, both parameters, the burning velocity and the cellular density, must be normalized between 0 and 1. Equation (3) shows the general formula used for normalization.

$$n_x = \frac{x_i - x_{min}}{x_{max} - x_{min}} \tag{3}$$

where x_i is the instantaneous value of the parameter being evaluated (S_n or ρ_{cell}), x_{max} is the maximum value achieved within the range of study, and x_{min} is the minimum value. In the case of the burning velocity, x_{min} corresponds to the laminar burning velocity (LBV) at that instant. The

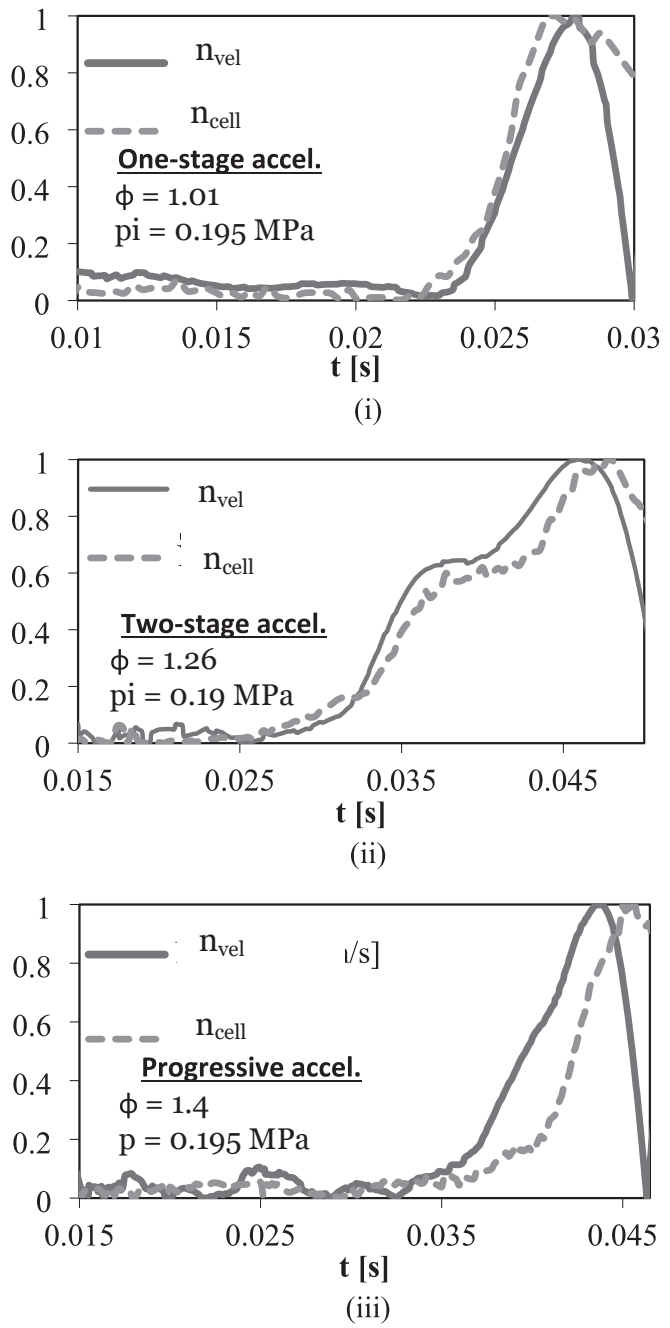

Fig. 8. Comparison between the normalized burning velocity and the normalized cellular density for the three different flame accelerations.

normalized parameters are identified as n_{vel} for the burning velocity and n_{cell} for the cellular density.

With the Schlieren imaging we have a 2D projection of a 3D flame, as a consequence the apparent size and shape of individual cells observed in the images are somehow distorted compared to the real ones in 3D. There are some works that have previously addressed this issue by applying image-processing techniques such as the one developed by Gu et al. [43] in 2021 and a more recent study carried out by Zhang et al. [44] in 2024. Such corrections are important when the study aims to obtain accurate absolute values of cell number or cell area. However, this study does not provide absolute quantification of the number of cells, because it focuses on the relative evolution of cellularity, with particular attention to the onset of quick growth. The use of a normalized cellular density index (n_{cell}) eliminates the projection effects and allows a robust comparison of relative changes during flame propagation

The results of the comparison between the normalized burning velocity and the normalized cellular density are presented below in Fig. 8 for the three experiments described in the previous section, which characterize the three types of acceleration (one-stage, two-stage and progressive).

The results presented in Fig. 8 show a clear relationship between the increase of the burning velocity (or acceleration) and the appearance of cellularity, as reflected by the cellular density. In all three experiments analysed, both parameters exhibit the same general trend. In the latter, a slight delay is observed between the increase in velocity and the development of cellularity; however, it is evident that both begin to rise at approximately the same time. This reinforces the hypothesis that the acceleration is caused by the onset of cellularity at the flame front and suggests that the evolution of cellularity determines the type of acceleration experienced by the burning velocity.

Once the hypothesis of cellularity is confirmed, i.e., a change in flame morphology, it is possible to define a ratio between the experimental burning velocity and the laminar burning velocity: the cellular burning stage, $CBS = S_{n,max}/LBV$, see Fig. 9.

The increase in the burning velocity due to cellularity increases the rate of heat release, as happens in internal combustion engines (ICE) with turbulence.

Another interesting parameter is the total increase in combustion velocity due to cellularity over time, referred to here as “cellular acceleration” (slope), which can be calculated as: $a_{cell} = \frac{u_{n,max} - LBV}{\Delta t}$. This parameter is represented in Fig. 10.

The results for both parameters —the cellular burning stage (CBS), and the cellular acceleration a_{cell} —are presented in Table 2 for each type of acceleration previously defined.

Analysing the results presented in Table 2, the values of the cellular burning stage (CBS) appear to be very similar across the three acceleration cases, approximately 1.4. However, when it comes to cellular acceleration (a_{cell}), significant differences are observed among the three values, with the one-stage type exhibiting a much higher acceleration, i.e. approximately 4.6 and 9.6 times greater than those of the other two, respectively. This implies that the one-stage type reaches the maximum value faster, whereas the two-stage and the progressive types are slower in doing so.

4. Conclusions

In the present work, the cellularity generated in ethanol flames and its effect on the burning velocity have been investigated.

For this study, several ethanol experiments were performed in a cylindrical constant volume combustion bomb, equipped with a system to visualize and record the evolution of the flame front. The initial temperature of all experiments was 343 K, while a range of initial pressures (0.15–0.30 MPa) and equivalence ratios (0.8–1.5) were tested. The experimental burning velocity results (u_n) were compared with the laminar burning velocity (LBV) obtained through kinetic modelling using CHEMKIN-PRO and the kinetic mechanism developed by Zhang et al. [1]. This comparison showed that the values of these two parameters were similar before the appearance of the cellular flame front. After that point, the burning velocity experienced an acceleration and diverged from the laminar burning velocity predicted by the kinetic model.

Results showed that there are three main types of acceleration the burning velocity can undergo due to cellularity: one-stage, two-stage, and progressive or multi-stage acceleration. The type of acceleration strongly depends on the flame equivalence ratio of the ethanol/air mixtures, which influences the burning velocity and the heat release rate, as also occurs with turbulence generation in internal combustion engines (ICEs). Additionally, the flame morphology varies depending on

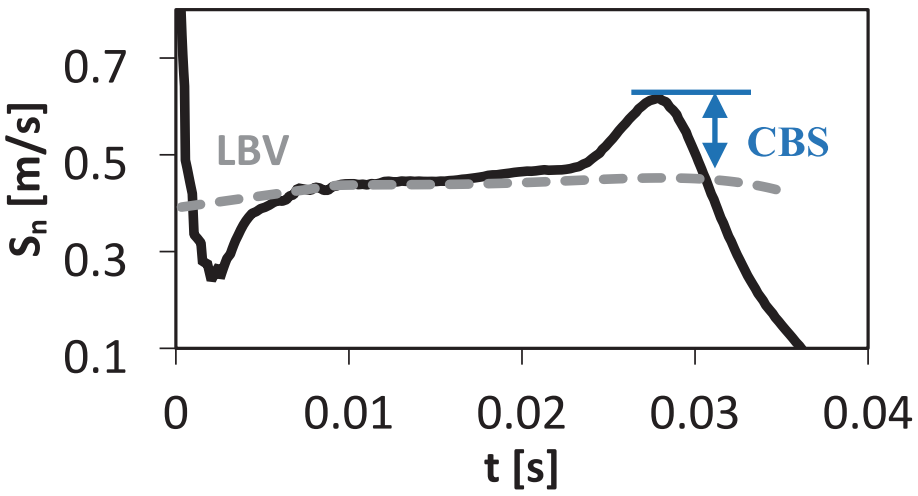

Fig. 9. Temporal evolution of the cellular burning rate (CBR).

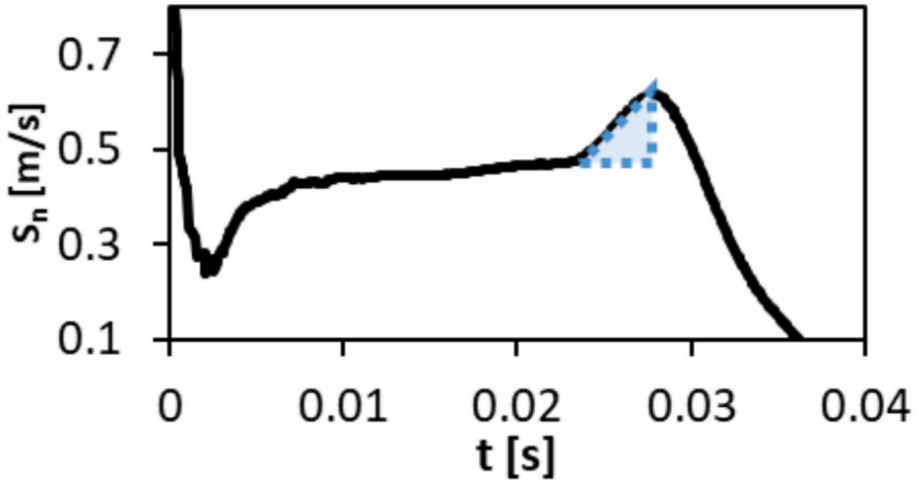

Fig. 10. Definition of the cellular acceleration for a burning velocity curve.

Table 2
Acceleration Types and the values of CBR and cellular acceleration.

One-stage acceleration		Two-stage acceleration		Progressive acceleration (multi-stage acceleration)	
p_i [MPa]/ φ	0.19/ 1.01	p_i [MPa]/ φ	0.19/ 1.26	p_i [MPa]/ φ	0.19/ 1.4
LBV [m/s]	0.444	LBV [m/s]	0.248	LBV [m/s]	0.132
$S_{n,max}$ [m/s]	0.617	$S_{n,max}$ [m/s]	0.349	$S_{n,max}$ [m/s]	0.181
CBS	1.390	***CBS***	1.406	***CBS***	1.370
a_{cell}[m/s^2]	34.551	a_{cell}[m/s^2]	7.429	a_{cell}[m/s^2]	3.598

the acceleration type: in one-stage acceleration, the cells are homogeneous, while in progressive acceleration, the cells are heterogeneous and clustered.

The role of cellularity in accelerating the burning velocity was confirmed by comparing the evolution of both the burning velocity and the cells.

Finally, two parameters were calculated to study the quantitative increase in burning velocity due to cellularity relative to the laminar value. These two parameters were the cellular burning stage (CBS) and the cellular acceleration. The CBS was similar across the three acceleration types, whereas the cellular acceleration reached its highest value in the one-stage acceleration, ~~was~~ intermediate in the two-stage, and the lowest in the progressive acceleration.

The richness of the mixture was found to enhance the onset of cellularity due to the greater tendency of rich mixtures to develop thermo-diffusive instabilities.

Funding statement

This research did not receive any specific grant from funding agencies in the public, commercial, or not-for-profit sectors.

CRediT authorship contribution statement

Miriam Reyes: Writing – review & editing, Writing – original draft, Validation, Supervision, Methodology, Investigation, Funding acquisition, Formal analysis, Conceptualization. **Rosaura Sastre:** Writing – original draft, Validation, Methodology, Investigation, Formal analysis, Data curation. **Hong-Quan Do:** Writing – original draft, Resources, Methodology, Investigation. **Luis Le Moyne:** Writing – review & editing, Validation, Supervision, Resources.

Declaration of competing interest

The authors declare the following financial interests/personal relationships which may be considered as potential competing interests: Miriam Reyes reports financial support was provided by University of

Valladolid. If there are other authors, they declare that they have no known competing financial interests or personal relationships that could have appeared to influence the work reported in this paper.

Acknowledgments

This work was developed with the support of the Research Group in Engines and Renewable Energies (MyER) from the University of Valladolid. The authors would like to thank the University of Valladolid (Spain) for financial support through the pre-doctoral contract CONTPR-2022-500.

The authors from the DRIVE Laboratory appreciate the financial support from the Council of Bourgogne-Franche-Comté. The authors would like to thank Dr. Luc-Sy Tran, PC2A Laboratory, CNRS, University of Lille for support in laminar burning velocity calculations.

A very special acknowledgement and expression of gratitude is dedicated to the memory of Benoite Lefort, who participated in this work and initiated the kinetic modelling at DRIVE Lab. but sadly passed away early in August 2024.

Data availability

Data will be made available on request.

References

[1] P. Dirrenberger, P.A. Glaude, R. Bounaceur, H. Le Gall, A.P. da Cruz, A.A. Konnov, F. Battin-Leclerc, Laminar burning velocity of gasolines with addition of ethanol, Fuel 115 (2014) 162–169.
[2] L.S. Tran, P.A. Glaude, F. Battin-Leclerc, Experimental study of the structure of laminar premixed flames of ethanol/methane/oxygen/argon, Combust. Explos. Shock Waves 49 (2013) 11–18.
[3] A.A. Konnov, A. Mohammad, V.R. Kishore, N.I. Kim, C. Prathap, S. Kumar, A comprehensive review of measurements and data analysis of laminar burning velocities for various fuel+air mixtures, Prog. Energy Combust. Sci. 68 (2018) 197–267.
[4] F.N. Egolfopoulos, D.X. Du, C.K. Law, A study on ethanol oxidation kinetics in laminar premixed flames, flow reactors, and shock tubes, Symp. (Int.) Combust. 24 (1992) 833–841.
[5] L. Sileghem, V.A. Alekseev, J. Vancoillie, E.J.K. Nilsson, S. Verhelst, A.A. Konnov, Laminar burning velocities of primary reference fuels and simple alcohols, Fuel 115 (2014) 32–40.
[6] L.F.M. Gárzon Lama, L. Pizzuti, J. Sotton, C.A. Martins, Experimental investigation of hydrous ethanol/air flame front instabilities at elevated temperature and pressures, Fuel 287 (2021) 119555.
[7] T. Li, X. Wang, Y. Ma, L. Wang, F. Oppong, C. Xu, G. Jiang, Investigation on hydrogen/ethanol intrinsic flame instability, Combust. Flame 241 (2022) 112064.
[8] F. Liu, Z. Liu, Z. Sang, X. He, M. Sjöberg, D. Vuilleumier, C. Liu, X. Li, Numerical study and cellular instability analysis of E30-air mixtures at elevated temperatures and pressures, Fuel 271 (2020) 117458.
[9] N. Zhang, Z. Fan, Z. Shenghui, P. Zhijun, Y. Jiangfei, L. Haifeng, C. Xu, Numerical and theoretical investigation of ethanol/air flame instability, Combust. Theor. Model. 24 (2020) 1108–1129.
[10] G. Broustail, F. Halter, P. Seers, G. Moréac, C. Mounaïm-Rousselle, Experimental determination of laminar burning velocity for butanol/iso-octane and ethanol/iso-octane blends for different initial pressures, Fuel 106 (2013) 310–317.
[11] M. Faghih, Z. Chen, The constant-volume propagating spherical flame method for laminar flame speed measurement, Sci. Bull. 61 (2016) 1296–1310.
[12] G.H. Markstein, Experimental and theoretical studies of flame-front stability, Dynamics of curved fronts, Elsevier, 1988, pp. 413-423.
[13] F. Oppong, Z. Luo, X. Li, Y. Song, C. Xu, Intrinsic instability of different fuels spherically expanding flames: a review, Fuel Process. Technol. 234 (2022) 107325.
[14] M. Matalon, Intrinsic flame instabilities in premixed and nonpremixed combustion, Annu. Rev. Fluid Mech. 39 (2007) 163–191.
[15] E. Robert, P.A. Monkewitz, Thermal-diffusive instabilities in unstretched, planar diffusion flames, Combust. Flame 159 (2012) 1228–1238.
[16] F. Williams, Combustion Theory, (1985), 412, The Benjamin/Cummings.
[17] V. Bychkov, M.A. Liberman, Dynamics and stability of premixed flames, Phys. Rep. 325 (2000) 115–237.
[18] A. Istratov, V. Librovich, On the stability of propagation of spherical flames, J. Appl. Mech. Tech. Phys. 7 (1966) 43–50.
[19] M. Matalon, The Darrieus–Landau instability of premixed flames, Fluid Dyn. Res. 50 (2018) 051412.
[20] N. Fogla, F. Creta, M. Matalon, Influence of the Darrieus-Landau instability on the propagation of planar turbulent flames, Proc. Combust. Inst. 34 (2013) 1509–1517.
[21] G. Troiani, F. Creta, M. Matalon, Experimental investigation of Darrieus–Landau instability effects on turbulent premixed flames, Proc. Combust. Inst. 35 (2015) 1451–1459.
[22] M. Reyes, F.V. Tinaut, B. Giménez, A. Camaño, Combustion and flame front morphology characterization of H_2–CO syngas blends in constant volume combustion bombs, Energy Fuel 35 (2021) 3497–3511.
[23] R. Addabbo, J. Bechtold, M. Matalon, Wrinkling of spherically expanding flames, Proc. Combust. Inst. 29 (2002) 1527–1535.
[24] C. Law, Propagation, structure, and limit phenomena of laminar flames at elevated pressures, Combust. Sci. Technol. 178 (2006) 335–360.
[25] D. Lapalme, F. Halter, C. Mounaïm-Rousselle, P. Seers, Characterization of thermodiffusive and hydrodynamic mechanisms on the cellular instability of syngas fuel blended with CH_4 or CO_2, Combust. Flame 193 (2018) 481–490.
[26] P. Clavin, F. Williams, Effects of molecular diffusion and of thermal expansion on the structure and dynamics of premixed flames in turbulent flows of large scale and low intensity, J. Fluid Mech. 116 (1982) 251–282.
[27] Y. Zhang, H. El-Merhubi, B. Lefort, L. Le Moyne, H.J. Curran, A. Kéromnès, Probing the low-temperature chemistry of ethanol via the addition of dimethyl ether, Combust. Flame 190 (2018) 74–86.
[28] S. Huang, R. Huang, P. Zhou, Y. Zhang, Z. Yin, Z. Wang, Role of cellular wavelengths in self-acceleration of lean hydrogen-air expanding flames under turbulent conditions, Int. J. Hydrogen Energy 46 (2021) 10494–10505.
[29] M. Reyes, R. Sastre, H.-Q. Do, B. Lefort, Impact of cellularity in the flame front on the burning velocity of ethanol/air flame in constant volume combustion bomb, Meas.: Sens. 38 (2025) 101721.
[30] F. Tinaut, M. Reyes, A. Melgar, B. Giménez, Optical characterization of hydrogen-air laminar combustion under cellularity conditions, Int. J. Hydrogen Energy 44 (2019) 12857–12871.
[31] M. Reyes, R. Sastre, F. Tinaut, J. Rodríguez-Fernández, Study and characterization of the instabilities generated in expanding spherical flames of hydrogen/methane/air mixtures, Int. J. Hydrogen Energy 47 (2022) 22616–22632.
[32] M. Reyes, F.V. Tinaut, A. Horrillo, A. Lafuente, Experimental characterization of burning velocities of premixed methane-air and hydrogen-air mixtures in a constant volume combustion bomb at moderate pressure and temperature, Appl. Therm. Eng. 130 (2018) 684–697.
[33] M. Reyes, F. Tinaut, Characterization of the burning velocity of hydrogen/methane blends in a constant volume combustion bomb, in: 2017 8th International Conference on Mechanical and Aerospace Engineering (ICMAE), 2017, pp. 257–261.
[34] M. Reyes, R. Sastre, B. Giménez, C. Sesma, Experimental, kinetic modeling and morphologic study of the premixed combustion of hydrogen/methane mixtures, Energies 15 (2022) 3722.
[35] A. Chemkin-Pro, Chemical Kinetics Simulation Software.
[36] Z. Wang, X. Han, Y. He, R. Zhu, Y. Zhu, Z. Zhou, K. Cen, Experimental and kinetic study on the laminar burning velocities of NH_3 mixing with CH_3OH and C_2H_5OH in premixed flames, Combust. Flame 229 (2021) 111392.
[37] J. Zhou, C. Lu, C. Xu, Z. Yu, Experimental and numerical study on the effect of hydrogen addition on laminar burning velocity of ethanol–air mixtures, Energies 15 (2022) 3114.
[38] A. Omari, L. Tartakovsky, Measurement of the laminar burning velocityusing the confined and unconfined spherical flame methods – a comparative analysis, Combust. Flame 168 (2016) 127–137.
[39] S. Huang, R. Huang, Y. Zhang, P. Zhou, Z. Wang, Z. Yin, Relationship between cellular morphology and self-acceleration in lean hydrogen-air expanding flames, Int. J. Hydrogen Energy 44 (2019) 31531–31543.
[40] Y.-H. Jiang, G.-X. Li, H.-M. Li, G.-P. Zhang, J.-C. Lv, Experimental study on the influence of hydrogen fraction on self-acceleration of H_2/CO/air laminar premixed flame, Int. J. Hydrogen Energy 45 (2020) 2351–2359.
[41] S. Yang, A. Saha, F. Wu, C.K. Law, Morphology and self-acceleration of expanding laminar flames with flame-front cellular instabilities, Combust. Flame 171 (2016) 112–118.
[42] R. Sastre, M. Reyes, J.M. Rodríguez-Díaz, J. Lacey, Characterization of cellular structure appearance in ethanol expanding spherical flames, Fuel 383 (2025) 133785.
[43] G. Gu, J. Huang, W. Han, C. Wang, Propagation of hydrogen–oxygen flames in Hele-Shaw cells, Int. J. Hydrogen Energy 46 (2021) 12009–12015.
[44] G. Zhang, H. Xu, D. Wu, J. Yang, M.E. Morsy, M. Jangi, R. Cracknell, W. Kim, Deep learning-driven analysis for cellular structure characteristics of spherical premixed hydrogen-air flames, Int. J. Hydrogen Energy 68 (2024) 63–73.